

Exploration of 2D Catalyst to investigate CO₂ reduction pathways computationally using Density Functional Theory based calculations.

A Thesis

submitted to

Indian Institute of Science Education and Research Pune

in partial fulfillment of the requirements for the

BS-MS Dual Degree Programme

by

Patil Durvesh Nitin



Indian Institute of Science Education and Research Pune

Dr. Homi Bhabha Road,

Pashan, Pune 411008, INDIA.

May, 2023

Supervisor: Dr Sailaja Krishnamurty (CSIR NCL Pune)

TAC Member: Dr Prasenjit Ghosh (IISER Pune)

© Patil Durvesh Nitin; 2023

All rights reserved

Certificate

This is to certify that this dissertation entitled **Exploration of 2D catalyst to investigate CO₂ reduction pathways computationally using Density Functional Theory based calculations** towards the partial fulfillment of the BS-MS dual degree programme at the Indian Institute of Science Education and Research, Pune, represents the work carried out by Patil Durvesh Nitin at the CSIR National Chemical Laboratory Pune, under the supervision of Dr Sailaja Krishnamurty, during the academic year 2022-2023.



Dr Sailaja Krishnamurty
Senior Principal Scientist, CSIR NCL Pune

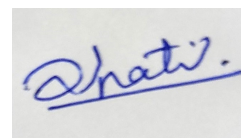
Committee

Supervisor: Dr Sailaja Krishnamurty

TAC Member : Dr Prasenjit Ghosh

Declaration

I hereby declare that the matter embodied in the report entitled Exploring 2D catalyst to study CO₂ reduction pathways using first principle calculations are the results of the work carried out by me at the CSIR NCL, Pune, under the supervision of Dr Sailaja Krishnamurty, and the same has not been submitted elsewhere for any other degree

A handwritten signature in blue ink, reading "Patil Durvesh Nitin", is shown on a light-colored background. The signature is written in a cursive style and is underlined.

Patil Durvesh Nitin

Acknowledgements

I am grateful to my supervisor Dr Sailaja Krishnamurty for allowing me to work under his supervision at CSIR NCL Pune. I thank my TAC member Dr. Prasenjit Ghosh for his valuable suggestions and comments during my mid-year evaluation. I would like to thank Dr. Aarti Shukla and labmates for guiding me throughout the project. I am also thankful to my friends Hrishikesh, Arsh, Sarang and my batchmates for their support throughout the journey. I would like to thank my friends and family for their encouragement and support throughout my studies. Finally, I would like to thank my parents. The special mention of the financial assistance provided by IISER Pune at crucial times which supported me a lot. Thanks to Chetan sir for guiding the process. I also acknowledge the computational facilities provided by IISER and NCL.

Abstract

Since the past century, extensive industrialization, power generation, and increased use of vehicles running on petroleum have led to a significant increase in greenhouse emissions. The natural phenomenon of greenhouse gases helps maintain a pleasant temperature suitable for life on earth due to the remissions absorbed by CO_2 and H_2O in the atmosphere. However, a staggering rise in CO_2 emissions has realigned the average global temperatures with an increase of more than 1oC , repercussions of which are being witnessed by several regions across the globe. In this thesis the CO_2 reduction pathways have been investigated on the two dimensional (2D) TiB_2 monolayer. C_1 products like formic acid, methanol, CH_4 production is investigated using the Density Functional Theory. The computational approach helps in predicting the performance of the catalyst in different environmental conditions. Density of states (DOS), and charge differences are also investigated to gain knowledge regarding the nature of adsorption at catalytic surface.

Contents

1	Introduction	9
1.0.1	Catalysis for CO ₂ RR	10
1.0.2	Electrochemical Reduction of CO ₂	11
1.0.3	2D Catalyst for CO ₂ RR	12
2	Theoretical Background and Computational Details	14
2.1	Many Body Schrödinger Equation	14
2.2	Born-Oppenheimer Approximation	15
2.3	Hohenberg Kohn Theorem	16
2.4	Kohn Sham Approach	18
2.5	Exchange and Correlation Energy	19
2.5.1	Self consistent cycle	20
2.6	Pseudopotential	20
2.7	Plane wave and Basis Sets	22
2.7.1	Computational Details	23
3	Results and Discussion	25
3.0.1	Crystal structure and electronic properties of TiB ₂ ML	25
3.0.2	CO ₂ adsorption on TiB ₂	27
3.0.3	CO ₂ to HCOOH pathways	29
3.0.4	Methanol Pathway	31
3.0.5	CH ₄ Pathways	31
4	Future Directions	34
4.0.1	Conclusion	34
4.0.2	Future Directions	34
4.0.3	Solvent Effect	35
4.0.4	External Potential	35

4.0.5 Doping	35
------------------------	----

List of Figures

1.1	Catalysis and effects on activation energy. This image is taken from https://doi.org/10.32657/10356/73265	10
1.2	Possible Pathways of CO ₂ RR. This image is taken from ref [27].	13
2.1	Many Body System to Electron Density. This figure is taken from https://doi.org/10.326572F1035	17
2.2	SCF cycle to arrive at a solution of KS Equations is described in the above Schematic Diagram	21
2.3	Pseudopotential Diagram[19]	21
3.1	Crystal structure of TiB ₂ monolayer. The purple and pink spheres represent the Ti and B atoms respectively.	26
3.2	(a) The Electronic Band structure of TiB ₂ (b) partial density of states (PDOS) of TiB ₂ ML. The zero energy is taken as the Fermi level.	26
3.3	Possible Pathways.[40]	27
3.4	Side view of most stable configurations from the Ti and B side of TiB ₂ monolayer. A) is the most stable configuration of CO ₂ adsorption on TiB ₂ ML from the Boron atom layer side and B) represents CO ₂ adsorption at the hollow site from the Ti side (The distance in the figure is in Angstroms)	28
3.5	(a) The most stable configuration of adsorbed CO ₂ on TiB ₂ , where bond lengths and angle are given in Å and (°). The purple, pink, yellow, and red spheres represent Ti, B, C, and O atoms. (b) The CDD diagram, where red and green regions represent the electron accumulation and depletion, respectively. The isosurface value is 0.008 e/Å ⁻³	28
3.6	HCOOH pathway on TiB ₂ surface	30
3.7	The free energy diagrams of CO ₂ RR to CH ₃ OH and corresponding intermediate configurations on TiB ₂ ML.	32
3.8	The free energy diagrams of CO ₂ RR to CH ₄ and corresponding intermediate configurations on TiB ₂ ML.	33

Abbreviations

- **ML** : Mono Layer
- **CO₂RR** : CO₂ Reduction
- **TM** : Transition Metal
- **CDD** : Charge Density Difference
- **HER** : Hydrogen Evolution Reaction
- **B_s** : Boron side
- **T_s** : Titanium Side
- **DFT** : Density Functional Theory

Chapter 1

Introduction

The industrial revolution's anthropogenic actions are responsible for the greenhouse effect and subsequent global warming. The unprecedented changes in global atmospheric CO₂ level are alarming signals for mankind and coming generations as it leads to various challenges and can create serious environmental problems for the coming generation. [27] Settling the growing energy needs of humans and simultaneously protecting the environment are the targets that need to be addressed. Climate change is primarily caused by our reliance on nonrenewable energy sources, particularly fossil fuels. As a result, we need alternative energy sources more than ever to ensure a viable future. Even though the development of renewable energy sources has advanced considerably, transporting renewable energy remains difficult and the source heavily influences the amount of energy generated.[17]

Scientists are developing strategies to mitigate the CO₂ level, which is the most important contributor to climatic changes such as global temperature and sea level rise.[1] Several strategies to mitigate the levels of CO₂ are discovered so far.[6, 38] Converting the CO₂ released from fossil fuel sources directly to some value-added products can be a sound strategy to resolve this problem. It can address clean energy generation and simultaneously mitigate the CO₂ level. In the previous decade, technology for carbon dioxide storage (CCS) was implemented as a strategy to store the atmospheric CO₂ artificially under pressure by developing the required technology. The storage cost and the safety issue caused by high-pressure storage were the key challenges faced in the CCS method of CO₂ capture. Another type of strategy includes Carbon Capture and Utilisation (CCU).[7, 1, 41] One of the most sought ways under this strategy is the use of various types of catalysts which can capture the atmospheric CO₂ emitted from its sources and convert to some value-added products. This can be the products that act as a precursor in the synthesis of various industrial reactions as well as an alternate source of fuels.

CO₂ reduction pathways to various C₁ products like Formic acid (HCOOH), Methanol(CH₃OH)

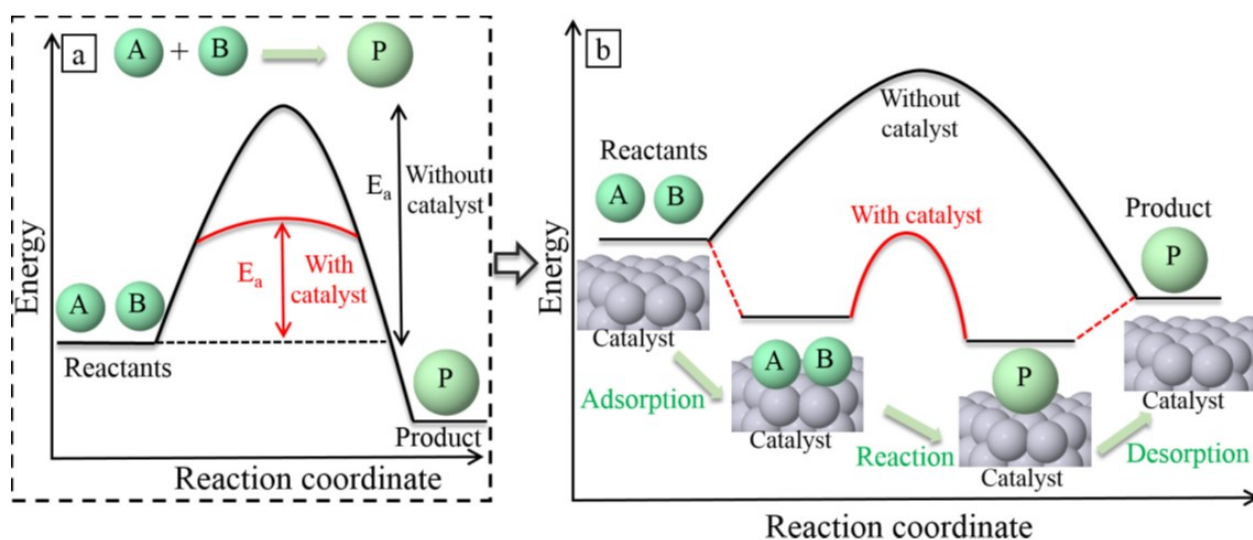


Figure 1.1: Catalysis and effects on activation energy. This image is taken from <https://doi.org/10.32657/10356/73265>

, Methane CH_4 , C_2 products like Ethanol ($\text{C}_2\text{H}_5\text{OH}$) are explored using different catalysts. [25, 27, 38, 32] Formic acid has a wider application in chemical industries and also it can act as a precursor for producing C_2 products like esters, ethanol is also predicted computationally. [24] There is a real test of the performance and the stability of the catalysts in C_2 products pathways as the C-C bond formation is a very tough task. Methanol being explored as an alternative to fossil fuels in vehicles is another value-added product getting attention [22]. The CO_2 reduction pathways are shown in Fig 1.2.

1.0.1 Catalysis for CO_2 RR

In CCU strategy discussed above, catalysis can act as a bridge between the CO_2 emitted to the value-added products. To facilitate the chemical reaction without getting adsorbed is the role of a catalyst in a chemical reaction. Baron was the person to coin this term way back in 1835. Depending on the phase of the reactants, Catalysis is classified into two types: Homogeneous Catalysis and Heterogeneous Catalysis. The diagram 1.1 describes the effect caused by catalyst in energetics of the reactions. In homogeneous Catalysis, the reactants,

and the catalyst are in the same phase while in heterogeneous Catalyst the reactants and the catalyst are present in a different phase. The metal-ligand complexes with metal centers like Ru, Re, Ir, etc are examples of some of the successful homogeneous catalysts for CO₂RR that are not cost-effective.[23] Usually, when it comes to bulk synthesis of products in the industry on a large scale heterogeneous catalysis is the preferred way. Photo-catalytic, thermal reduction, reduction by using radiations, Electrochemical reduction, etc are several ways which are tested for capturing the CO₂[41, 27, 32] In the thermal reduction of CO₂, creating surroundings of high pressure and temperature and thermal stability of catalyst to withstand the high temperatures were some of the issues witnessed in these methods. Electrochemical conversion is the most sought option for CO₂RR due to the ability to generate cost-effective catalysts, and the ability to induce many new properties on the electrode surface which give captivating results in overall catalytic activity. Though many catalysts successfully demonstrate the CO₂RR but the efficiency, productivity, and stability of catalysts are not significant enough to consider these catalysts for industrial purposes on large scale. One of the major reasons for the challenges is the stability of the CO₂ molecule itself. It is extremely difficult to break the covalent bond between carbon and oxygen which increases the energy requirement for its hydrogenation. This creates the situation of high overpotential for the reactions.[32] Another reason is the competitive reactions that are possible. To develop a good catalyst for CO₂RR it is also important to investigate the ability of catalysts to suppress the competitive reaction. In this case, it is the Hydrogen Evolution Reaction.[29, 32]

1.0.2 Electrochemical Reduction of CO₂

Electrochemical reduction of CO₂ has attracted a lot of attention in recent times. Many works are being carried out in designing efficient catalysts which increase the adsorption of CO₂ on the catalytic surface. The two-dimensional (2D) materials with metal centers are being explored in a wide range due to the possibility of better adsorption of CO₂ molecule on the catalytic surface. CO₂RR comes with the challenges like high overpotential, competitive reactions like Hydrogen-Evolution Reaction(HER), lower current efficiency, and many more. Due to reactions like HER, the presence of active sites on catalysts becomes extremely crucial which increases the affinity for CO₂ reduction compared to HER.[25, 32] In the electrochemical reduction of CO₂ usually, CO₂ is added at the cathode. The electrode potential has a significant impact on how the CO₂ electro-reduction product is composed. Other significant variables influencing selectivity include binding species and the thermodynamic potential difference of intermediates.

Here, we are trying to reduce the CO_2 molecule which is in the gaseous phase on a 2D catalyst that is solid in nature. So, the electrochemical reduction using an electrocatalyst is the process of heterogeneous catalyst as our reactants and 2D sheet are in a different phase. To withstand extreme conditions, heterogeneous catalysis has become a popular tool in electrochemical conversion reactions. [23] The energy cost required to initiate any reaction is reduced significantly due to the introduction of a catalyst. Now, let us see some of the works on designing of electrocatalysts for CO_2RR and converting them into value-added products.

1.0.3 2D Catalyst for CO_2RR

2D catalysts were explored on a wide scale to study the CO_2RR pathways and demonstrated the production of various C_1 as well as CO_2 products some works successfully demonstrated MoTe_2 as a promising catalyst. One of the difficulties with this kind of catalyst is that the catalytic activity depends on the size of the nanosheets.[12] The inertness of the atoms located at the basal planes Some works demonstrated the use of Graphene by introducing defects using metal centers on the surface as a catalytic surface.[4, 15] Introducing defects in graphene by various metal centers were incorporated to synthesize single-atom catalysts(SACs), etc. The Boron-nitride (BN) layers which are analogous in structure to Graphene are also explored for CO_2 reduction purposes. Several studies have also been tried to introduce metal clusters on such 2D surfaces to generate an active site for activating the CO_2 molecule.[15] Still, the thermodynamic stability of the intermediates and overpotential remains the challenge for these materials also. Many metals like Cu, Au, Ag, Ni, Pt, Rh, Pd, etc have been investigated as potential electrocatalysts. Among this list, Cu usually has topped the list in terms of catalytic performance and affinity for adsorption of CO_2 . But the major concern regarding Cu is noticed that it also shows the affinity of HER reaction. So, the inability to suppress the competitive reaction is the major challenge in CO_2RR . Transition Metal(TM) diborides are a class of 2D catalysts which have been reported in various electro-catalyst applications like Nitrogen Reduction Reaction (NRR). This family includes TiB_2 , VB_2 , HfB_2 etc.[35] From the above discussion, we noticed the importance of the presence of active centers on the catalytic surface and due to the presence of metal surface alternate to hexagonal Boron lattice, we anticipate TM Diborides to show amazing results in CO_2RR also. For this, we have chosen to study the CO_2RR on TiB_2 monolayer (ML). The synthesis of TM Diborides are also reported in several studies [11, 37, 36].

We will be studying the CO_2 reduction pathways on TiB_2 ML. Bulk TiB_2 is observed to have high thermal stability and electrical conductivity. The TiB_2 ML can be exfoliated from

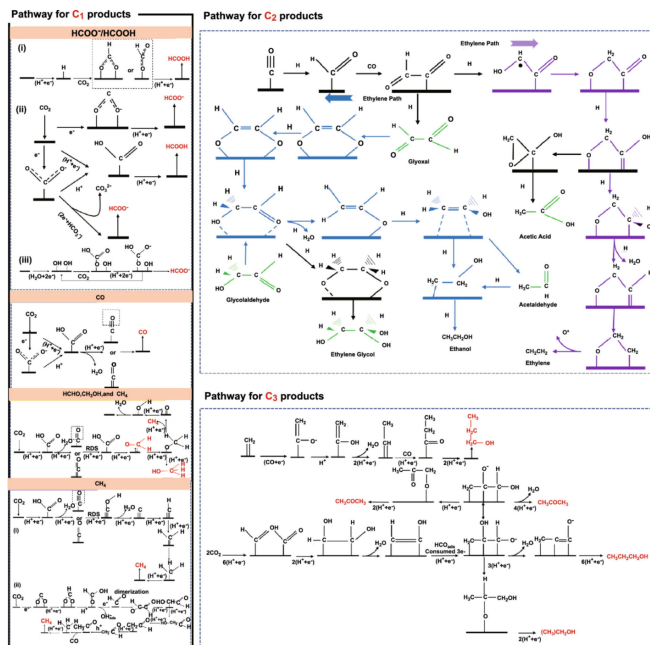


Figure 1.2: Possible Pathways of CO₂RR. This image is taken from ref [27].

the Bulk TiB₂ structures. TiB₂ belongs to the class of Metal Diborides.[35] The metal centers above the hexagonal metal lattice which are covalently bounded separate the two B-atom layers. In the case of TiB₂ due to presence of Ti atoms containing unpaired *d* electrons give rise to some diverse remarkable physical properties. Very high melting points, resistance to oxidation, corrosion, and hardness were some of the key properties of TiB₂. Some works have also reported the successful synthesis of TiB₂ nanoparticles and nanoribbons.[3] Due to the presence of transition metal centers on TiB₂ good charge transfer properties are predicted in the previous theoretical investigations of the TiB₂ monolayer.

Chapter 2

Theoretical Background and Computational Details

In our study of exploring CO₂RR pathways, we have used the Density Functional theory, a very popular computational tool, to solve computational chemistry problems. In the past few decades, DFT is also been widely used in applications of heterogeneous catalysis. It helps in reducing the problem of solving the Schrodinger equation in 3N coordinates to equation of three coordinates. It reduces the computational cost significantly. The results obtained from DFT studies have also shown consistency with the experimental studies' data. Various studies can be done by using DFT such as magnetic properties, predicting active sites on catalysts, electronic band structures, the density of states, etc. We will begin by understanding the basic many-body Schrodinger equation.

2.1 Many Body Schrödinger Equation

We have a system with N nuclei and n electrons. The Time Independent Schrödinger equation can be represented as

$$\hat{H}\psi = E\psi \tag{2.1}$$

here, $\Psi(\mathbf{R}, \mathbf{r})$ is the many body wavefunction. The Hamiltonian of the system is represented as

$$\hat{H}_{tot} = -\sum_{I=1}^N \frac{\hbar^2}{2M_I} \nabla_I^2 - \sum_{i=1}^n \frac{\hbar^2}{2m_e} \nabla_i^2 + \frac{e^2}{2} \sum_{I=1}^N \sum_{I \neq J}^N \frac{z_I z_J}{|\mathbf{R}_I - \mathbf{R}_J|} + \frac{e^2}{2} \sum_{i=1}^n \sum_{i \neq j}^n \frac{1}{|\mathbf{r}_i - \mathbf{r}_j|} - e^2 \sum_{I=1}^N \sum_{i=1}^n \frac{z_I}{|\mathbf{R}_I - \mathbf{r}_i|}, \tag{2.2}$$

The ground state energy is time-independent, so it is known as Time Independent Schrödinger

Equation.[31] Initial two terms in the above many-body equation represent the KE of the nuclei and electrons of the system respectively. Coulombic interactions between nuclei-nuclei, electron-electron, and electron-nuclei are denoted by the third, fourth, and fifth terms of the above equation. M_I and m_e represent the masses of I th nuclei and electrons respectively. The problem arises in solving the 4th and 5th terms of the TISE equation which are non-local terms.

2.2 Born-Oppenheimer Approximation

The Hamiltonian for the above many-body Schrödinger Equation can be written as

$$\hat{H}_{tot} = T_n + T_e + V_{nn} + V_{ee} + V_{ne} \quad (2.3)$$

we have the terms which denote the electron-electron, internuclear and electron-nuclei interaction. and Here, T_n stands for nuclear kinetic energy, T_e for electron kinetic energy, and V_{nn} , V_{ee} , and V_{en} for nuclear kinetic energy, electron kinetic energy, and nuclear kinetic energy, respectively. The mass of the nucleus is nearly 2000 times that of an electron due to which the speed of nuclear motion is relatively slower we can assume the nuclear motion to be stationary compared to the electron. This is known as Born-Oppenheimer Approximation. Thus we can assume T_n and V_n as constant For the fixed value of \mathbf{R} . So Hamiltonian of the system can be denoted as the addition of \hat{H}_e and \hat{H}_n denoting the electronic and nuclear components.

$$H_{tot} = H_n + H_e \quad (2.4)$$

where

$$\hat{H}_e = T_e + V_{ne} + V_{ee} \quad (2.5)$$

H_e has a parametric dependence on the nuclear coordinates and function of electronic coordinates.

$$\hat{H}_n = T_n + V_{nn} \quad (2.6)$$

H_n is only dependent on nuclear coordinates.

Due to this approximation, it is possible to decouple the total wavefunction $\Psi(\mathbf{R}, \mathbf{r})$ into the electronic($\psi(\mathbf{R}, \mathbf{r})$) and nuclear ($\Phi_n(\mathbf{R})$) components.

$$\Psi(\mathbf{R}, \mathbf{r}) = \sum_n \Phi_n(\mathbf{R})\psi_n(\mathbf{R}; \mathbf{r}) \quad (2.7)$$

Thus, the electronic part of the Schrodinger equation becomes

$$\hat{H}\Psi_e(\mathbf{R}, \mathbf{r}) = E_e(\mathbf{R}, \mathbf{r})\psi_e(\mathbf{R}; \mathbf{r}) \quad (2.8)$$

In the presence of this constant nuclear potential, we can assume the nuclei as being fixed in space and solve for the electronic wave function. Instead of attempting to solve for the simultaneous motion of both electrons and nuclei, which would necessitate a far more difficult computation, this is significantly simpler. After the application of the Born-Oppenheimer Approximation, still we need to deal with the 3N variable equation and terms like electron-electron repulsion interaction are present which are non-local in nature hence due to which its difficult to solve the many-body Schrödinger equation.[13] we need a change in approach to solve this problem.

2.3 Hohenberg Kohn Theorem

The Hohenberg-Kohn theorems have significant effects on how quickly DFT computations may be completed. DFT calculations become more computationally effective and enable the prediction of the electronic structure and characteristics of materials and molecules in larger and more complex systems by downsizing the challenge of solving for the electronic wave function to solving for the electron density. 2.1 illustrates the schematic of replacing the many body system with the density.

$$\hat{H}_{tot}\Psi(\mathbf{R}, \mathbf{r}) = E_{tot}\Psi(\mathbf{R}, \mathbf{r}) \quad (2.9)$$

Theorem1- *The external potential V_{ext} is a unique functional of $n(r)$ since, in turn V_{ext} fixes \hat{H} we see that the full many particle ground state is a unique functional of $n(r)$ [28]*

The first theorem states that there exists a one-to-one mapping between the external potential and the electron density which means that different values of external potential cannot give the same value of ground state electron density. There exists unique V_{ext} for ground state electron density.

Theorem2- *The electron density that minimizes the energy of the overall function is the true electron density corresponding to the full solutions of the Schrödinger equation[28]*

According to the 2nd Hohenberg-Kohn theorem, the overall ground-state energy can be attained by the universal functional of the electron density. This functional solely depends on the electron density and is not reliant on the particular form of the external potential. As a result, the system's overall energy can be represented as a function of the electron density.[13]

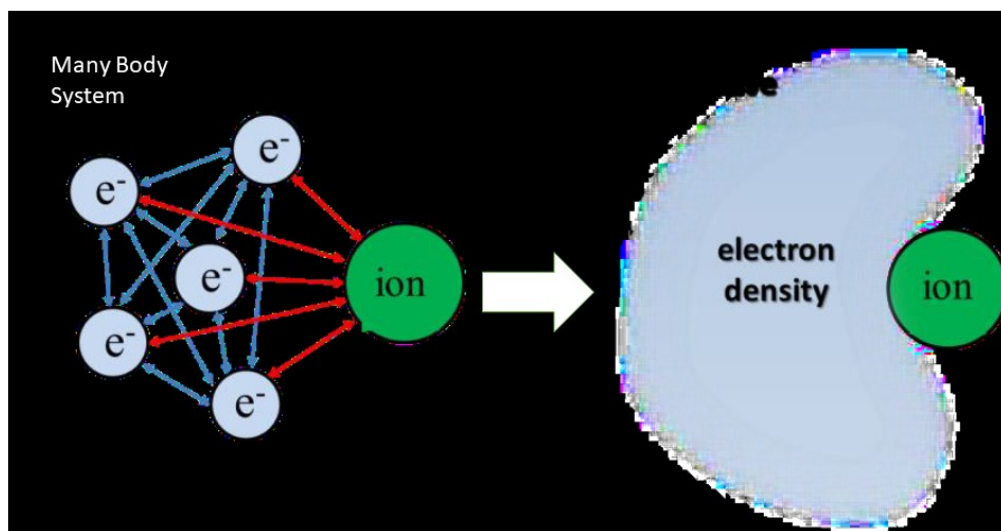


Figure 2.1: Many Body System to Electron Density. This figure is taken from <https://doi.org/10.326572F103562F73265>

Hohenberg Kohn Functional for any external potential V_{ext} can be stated as

$$E^{HK}[n(r)] = F^{HK}[n(r)] + \int V_{ext}(\mathbf{r})n(\mathbf{r})d\mathbf{r}, \quad (2.10)$$

where $F^{HK}[n(r)]$, is the sum of the K.E. of the electrons ($T[n(r)]$) and the electron-electron interaction ($E_{ee}[n(r)]$) terms, can be stated as:

$$F^{HK}[n] = T[n(r)] + E_{ee}[n(r)]. \quad (2.11)$$

This universal functional operates only on density. These theorems do not offer a meaningful (acceptable) mathematical formulation of the universal functional F^{HK} in terms of density. As a result, it is still challenging to solve the Schrödinger equation.

2.4 Kohn Sham Approach

A method to address the issue of solving the unknown functional was presented in 1965 by Kohn and Sham, allowing one to convert the precise ground state density of an interacting system to the ground state density of a hypothetical system of non-interacting particles. A collection of independent particle equations that can be solved numerically are provided by this technique.[14] It is assumed that a hypothetical non-interacting electron system has a density equal to that of interacting electrons. Finding a hypothetical system of non-interacting electrons with the same density as the "real" one with interacting electrons becomes the difficulty, rather than solving for the universal H-K functional. The Hamiltonian operator for the fictitious non-interacting electron system with V_r as the local potential for each component of the system:

$$\hat{H}_s = -\frac{\nabla^2}{2} + V_r(\mathbf{r}) \quad (2.12)$$

By the KS approach, the universal functional can be written as

$$F_{KS}[n(r)] = T_o[n(r)] + E_H[n(r)] + E_{XC}[n(r)], \quad (2.13)$$

$T_o[n(r)]$, $E_H[n(r)]$, $E_{XC}[n(r)]$ represents the KE, Hartree energy, and correlation energy respectively. $T_s[n(r)]$ is not the same as that of KE of interacting systems. $T_s[n(r)]$ can be written as

$$T_o[n(r)] = \frac{1}{2} \sum_i \int |\nabla\psi_i(\mathbf{r})|^2 d\mathbf{r}. \quad (2.14)$$

Hartree energy $E_H[n]$ is written as

$$E_H[n] = \frac{1}{2} \int \int \frac{n(\mathbf{r})n(\mathbf{r}')}{|\mathbf{r} - \mathbf{r}'|} d\mathbf{r}d\mathbf{r}', \quad (2.15)$$

$n(\mathbf{r})$ is the charge density which is written as:

$$n(\mathbf{r}) = \sum_{i=1}^n |\psi_i(\mathbf{r})|^2. \quad (2.16)$$

Finally, the KS Functional is represented as,

$$E_{KS}[n] = F_{KS}[n] + \int n(\mathbf{r})V_r(\mathbf{r})d\mathbf{r}. \quad (2.17)$$

KS potential as a function of charge density is given by

$$V_{KS}(\mathbf{r}) = V_{\text{ext}}(\mathbf{r}) + \int \frac{n(\mathbf{r}')}{|\mathbf{r} - \mathbf{r}'|} d\mathbf{r}' + V_{XC}(\mathbf{r}), \quad (2.18)$$

V_{XC} is the functional derivative of the Exchange Correlation energy term.[10] The Final KS equation reduces to

$$\left(-\frac{\hbar^2}{2m_e} \nabla^2 + V_{KS}(\mathbf{r}) \right) \psi_i(\mathbf{r}) = \epsilon_i \psi_i(\mathbf{r}). \quad (2.19)$$

2.5 Exchange and Correlation Energy

Different approximations for the exchange-correlation (xc) functional are suggested in order to achieve the desired balance between accuracy and computational cost because the analytical form of exchange-correlation energy is unknown. Generalized gradient approximation (GGA), local density approximation, and meta-GGA are three examples of local and semi-local approximations. Non-local approximations include hybrid functionals and random phase approximations. The energy of exchange-correlation turns into a local function in the limit of a uniform electron gas. The local density approximation is thus the first and most basic exchange-correlation functional of the Kohn-Sham technique. LDA is represented as

$$E_{XC}^{LDA} = \int n(\mathbf{r})\epsilon_{XC}^{hom}(n(\mathbf{r}))d^3\mathbf{r} \quad (2.20)$$

It is assumed that density changes gradually with a position in this instance. As a result, the exchange-correlation energy per electron is exclusively dependent on electron density,

disregarding its derivatives. From Pauli Exclusion Principle, we know that two electrons with the same spin cannot acquire the same state hence electrons with similar spins will repel each other. While applying LDA, we consider homogeneous electron gas in which this term is approximated.[18] The electrons being negatively charged and their interactions with each other are responsible for the origin of this term. The difference in kinetic energy of interacting and non-interacting system mainly contribute to this part. LDA is effective for systems similar to homogeneous gas, such as metals, but it fails for inhomogeneous systems, such as atoms and molecules. This can be used to describe the atomic structures, elastic characteristics, and vibrational properties for a variety of systems. However, reliable predictions of the energetics of chemical bonds, binding energy, reaction temperatures, and activation energy barriers are not possible. Both the electronic density and the $\Delta n(\mathbf{r})$ at a given site have been taken into consideration in subsequent efforts to increase exchange-correlation energy. The generalised gradient approximation (GGA) is the name of this semi-local approximation.[5]GGA is represented mathematically as

$$E_{XC}^{GGA} = \int n(\mathbf{r})\epsilon_{XC}(n(\mathbf{r}), |\nabla n(\mathbf{r})|)d^3\mathbf{r} \quad (2.21)$$

LDA usually performs well when the pace of variation in density is less. But to take account of inhomogeneity is also taken care of due to the inclusion of the gradient term of the electron density. Here, we have used the Perdew, Burke, Erzenhof exchange-correlation energy functional due to its better representation of a many-body system compared to LDA.[21].

2.5.1 Self consistent cycle

2.6 Pseudopotential

The valence electrons which are loosely held are mostly responsible for most of the physical properties. The core electrons do not show involvement in the bonding. Loosely held valence electrons oscillate near core region So, can ignore the effect of core electrons by introducing a 'Pseudopotential'.Pseudopotentials simplify the calculation of the electronic structure by replacing the full nuclear potential energy with a simpler potential energy that only includes the effect of the core electrons. [20] There are two types of pseudopotentials: norm-conserving and ultrasoft. Norm-conserving pseudopotentials are designed to conserve the norm of the wave function, which ensures that the total number of electrons in the system is conserved. Ultrasoft pseudopotentials are more flexible and allow for a better description of the valence electrons.Diagram of the concept is replicated in the fig. 2.3

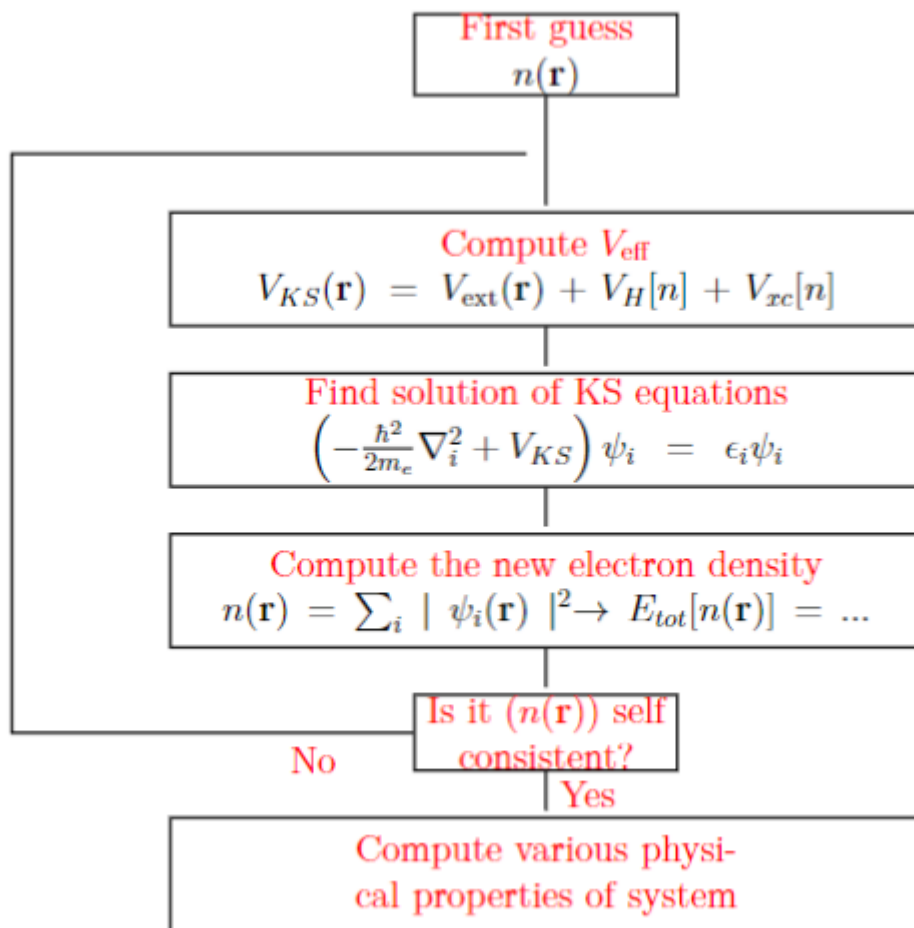


Figure 2.2: SCF cycle to arrive at a solution of KS Equations is described in the above Schematic Diagram

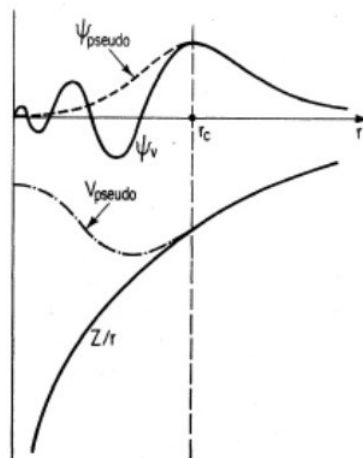


Figure 2.3: Pseudopotential Diagram[19]

2.7 Plane wave and Basis Sets

Because there are an infinite number of electrons in the system, a wave function must be computed for each one. Additionally, because each electronic wavefunction covers the entire solid, an infinite basis set is needed to expand each wavefunction. Calculations on periodic systems and the application of Bloch's theorem to the electronic wave function can be used to solve both of these issues. The electronic wave function is represented as

$$\psi_k(r) = e^{i\mathbf{k}\cdot\mathbf{r}} u_k(r) \quad (2.22)$$

where $u_k(r)$ is a basis set function with a periodicity equal to that of the supercell. $u_k(r)$ can be represented as

$$u_k(r) = \frac{1}{V} \sum_{\mathbf{G}} C_{\mathbf{k},\mathbf{G}} e^{i\mathbf{k}\cdot\mathbf{G}} \quad (2.23)$$

$$(2.24)$$

where \mathbf{G} represents the reciprocal lattice vectors of the system. n and k denote the band index and wavevector in the first Brillouin zone, respectively. n_1, n_2, n_3 can be any integers. Therefore, the Kohn-Sham equations can be separately solved for each value of k using periodicity. The reciprocal space is the space of the k vector (also called momentum space or k -space). The values of k are chosen to be within the first Brillouin zone, a primitive cell of the reciprocal lattice (BZ). Different methods of dividing BZ for the k -mesh are possible. So, instead of computing for an infinite no of plane waves taking account of only plane waves within the primitive cell will make the computation lot easier and faster. So to get rid of plane waves with higher values of \mathbf{G} we use the E_{cut} to truncate the basis set to a converged value at a cutoff value. [20] It solves the problem of solving for infinite basis set E_{cut} is denoted by

$$E_{cut} = \frac{\hbar^2 |\mathbf{k} + \mathbf{G}|^2}{2m} = \frac{\hbar^2 \mathbf{G}_{cut}^2}{2m} \quad (2.25)$$

The challenge of

By incorporating the concept of E_{cut} the final equation of representing the infinite sum of plane waves becomes

$$\psi_k(r) = \frac{1}{V} \sum_{|\mathbf{k} + \mathbf{G}| \leq \mathbf{G}_{cut}} C_{\mathbf{k},\mathbf{G}} e^{i(\mathbf{k} + \mathbf{G})\cdot\mathbf{r}} \quad (2.26)$$

2.7.1 Computational Details

Density functional theory-based first-principles calculations have been performed using by Quantum ESPRESSO package [8]. The generalized gradient approximation (GGA) is used to describe the exchange-correlation energy functional parameterized with Perdew, Burke, and Ernzerhof [21]. The electron-ion interaction are incorporated by using ultrasoft pseudopotentials [30] in which the valence electrons are : Ti $3d^2, 4s^2, 4p^0$, B: $2s^2, 2p^1$. C: $2s^2, 2p^2$, O: $2s^2, 2p^4$ and H: $1s^1$, We have used 50 Ry for the kinetic energy cutoffs and 480 Ry for the charge density cutoffs. The Brillouin zone (BZ) integration is performed with $(12 \times 12 \times 1)$ Monkhorst–Pack [16] k-points grid for the unit cell of TiB_2 and $(3 \times 3 \times 1)$ for the supercell of TiB_2 . We have incorporated Grimme-D2 corrections in all the calculations to account for long-range correlation effects between adsorbed species and adsorbent. A vacuum of more than 12\AA is maintained along the z-axis to avoid the interactions between the atomic layers of the consecutive supercells. We have used Gaussian smearing of 0.005 eV to speed up convergence.

The adsorption energies (E_{ads}) of CO_2 molecules and other intermediates are calculated using Eqn.

$$E_{ads} = E_{I+\text{TiB}_2} - E_{\text{TiB}_2} - E_I \quad (2.27)$$

where $E_{I+\text{TiB}_2}$, E_{TiB_2} and E_I are the total energy of adsorbed intermediates and catalyst (TiB_2 ML), the total energy of catalyst and total energy of intermediates respectively.

The change in Gibbs free energy (ΔG) for each CO_2 reduction step is calculated using the computational hydrogen electrode (CHE) model, in which it is assumed that $(\text{H}^+ + \text{e}^-)$ transfers in each elementary step. The (ΔG) of each state is obtained by using the eqn. 2.28 at electron potential $U = 0$ (versus the reversible hydrogen electrode (RHE)).

$$\Delta G = \Delta E + \Delta ZPE + \int C_p dT - T\Delta S \quad (2.28)$$

where ΔE is electronic energy taken from DFT calculation, ΔZPE , $\int C_p dT$, and ΔS are the zero point energy(ZPE) difference, enthalpic temperature correction (from 0 to T K) and the entropy difference between the products and the reactants, which are calculated by vibrational frequency. The T is the temperature and is set at $T = 298.15\text{K}$. Limiting potential (U_L) is defined as the minimum applied potential after which every step of electrochemical reaction to being exothermic. The U_L is calculated as :

$$U_L = -\frac{\Delta G_{max}}{e} \quad (2.29)$$

where ΔG_{max} is the free energy change of the potential limiting step (PLS) in reduction

reaction at 0 V vs RHE

The charge density difference (CDD) is calculated as follows:

$$\Delta(\rho) = \rho_{I+TiB_2} - \rho_{TiB_2} - \rho_I \quad (2.30)$$

where ρ_{I+TiB_2} , ρ_{TiB_2} , and ρ_I are the total charge densities of the ML after the intermediate adsorption, the isolated TiB_2 ML, and the isolated intermediates, respectively.

Chapter 3

Results and Discussion

3.0.1 Crystal structure and electronic properties of TiB₂ ML

In bulk TiB₂, One Ti atom is coordinated with six B atoms, and one B atom is coordinated with three Ti atom. 2 B atoms and one Ti atom comprises one unit cell of TiB₂. The B atoms are located in a hexagonal lattice with Ti atoms located in the center as shown in Fig. 3.1. The B-B bond distance in bulk TiB₂ is found to be (1.73Å) and the interplanar distance between Ti and B layer is (1.575Å). It crystallizes in *P6/mmm* space group.

We are exploring TiB₂ monolayer as a potential 2D material for the application of carbon dioxide reduction to some value-added products. The TiB₂ monolayer can be considered as a layer exfoliated from bulk TiB₂. It has C_{6v} point group symmetry. TiB₂ monolayer can be considered as a single layer exfoliated from the bulk TiB₂. Some of the reports have also reported the successful synthesis of TiB₂ nanosheets.[3] As shown in fig.3.1 the unit cell of TiB₂ contains 2 B atoms and one Ti atom. Initially, we performed the spin-polarized relax calculations to obtain the optimized structure of TiB₂. The energy value obtained from relax calculations ensures in It has a honeycomb-like structure and the lattice parameter a=b= 3.17Å which we obtained from our calculations. The B-B bond length is 1.80 Å and the interplanar distance between Ti and B or the thickness(h) is 1.20Å. We found that the thickness(h) in the TiB₂ monolayer is less compared to that of Bulk TiB₂ which denotes the

Table 3.1: The calculated lattice parameters, bond length, thickness of the MB₂ ML.

	system	lattice parameter	B-B
Present work	TiB ₂ (bulk)	3.121(3.126)	1.80
Present work	TiB ₂ (ML)	3.121(3.126)	1.80
Other work	TiB ₂ (bulk)	3.121(3.126)[37]	1.80
Other work	TiB ₂ (ML)	3.121(3.126)[37]	1.80

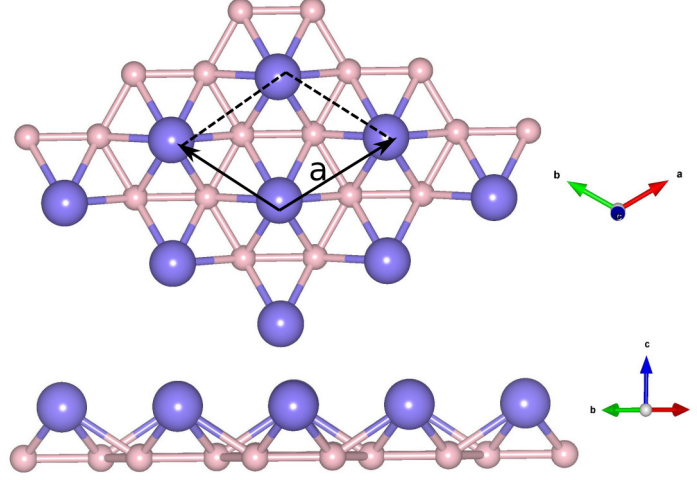


Figure 3.1: Crystal structure of TiB_2 monolayer. The purple and pink spheres represent the Ti and B atoms respectively.

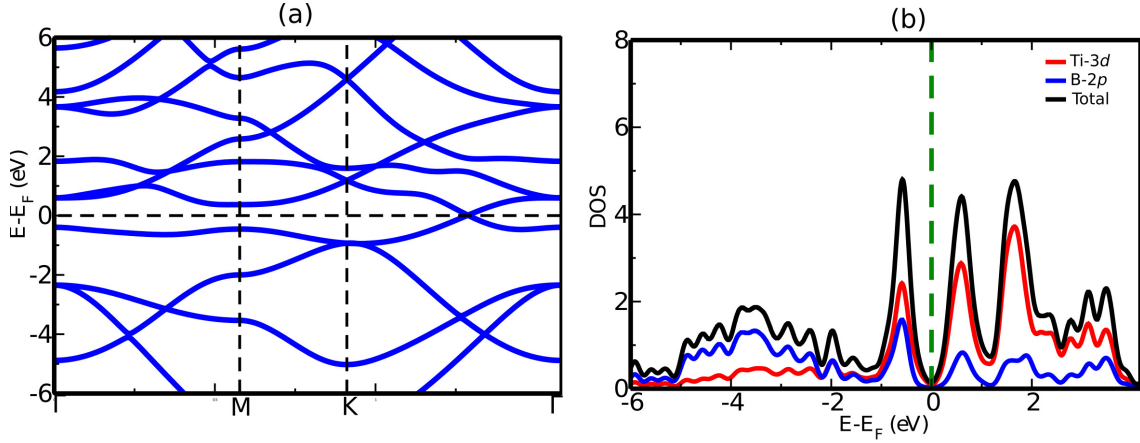


Figure 3.2: (a) The Electronic Band structure of TiB_2 (b) partial density of states (PDOS) of TiB_2 ML. The zero energy is taken as the Fermi level.

stronger interplanar interactions between the Ti atoms and the B atoms. The values obtained from our calculation are found to be consistent with the previous studies of TiB_2 [39]. The electronic band structure and partial density of state (PDOS) of the TiB_2 is shown in Fig. 3.2. From band structure calculation, we find that it is metallic in nature. Further, near the Fermi level primarily the hybridized of Ti- d and B- p orbitals are contributed.

The PDOS plots depict that the states near the Fermi level are due to the contribution of hybridized Ti- d and B- p electrons which confirms that TiB_2 is, metallic in nature. The crossover of the states between the κ and Γ denotes the Dirac states analogous to that of Graphene which is due to the Ti d electrons.[39]. Additionally, we have also calculated the electronic band structure to get insights into the electronic properties. The electronic band

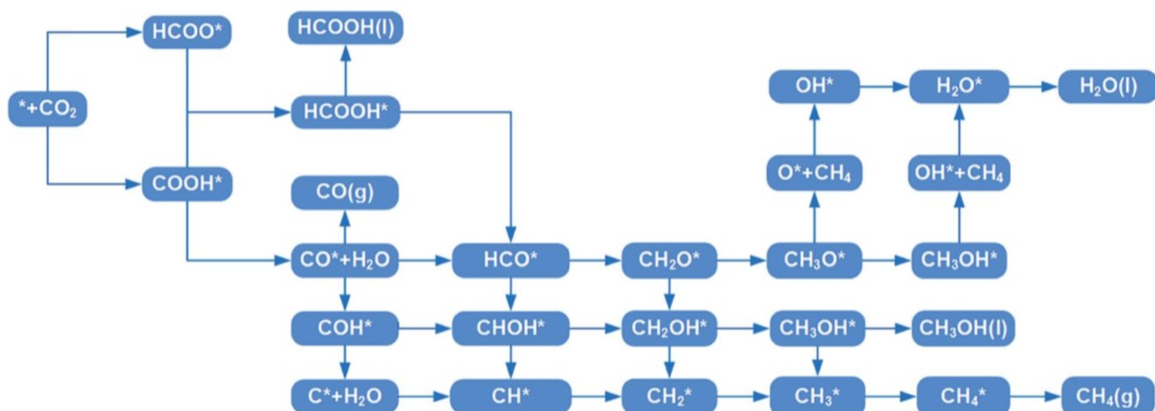


Figure 3.3: Possible Pathways.[40]

structure also confirms that TiB_2 is metallic in nature and is anisotropic mainly due to the states near the Fermi level. [26]. From structural properties it's clear that TiB_2 monolayer is a 2D planar surface and electronic properties confirm the presence of states near the Fermi level which are the main reason for choosing TiB_2 as a catalyst for exploring CO_2RR pathways. The following is a flow chart of possible pathways in obtaining HCOOH , CH_3OH and CH_4 as our value added products. The schematic of our pathways are shown in the above diagram 3.3

3.0.2 CO_2 adsorption on TiB_2

The very first step in CO_2 reduction reaction is the capture and activation of CO_2 molecule on the catalyst surface. The ground state of neutral CO_2 molecule has linear geometry with a C-O bond length of 1.17 Å. The bent geometry of CO_2 is formed when it is chemisorbed on the surface with the formation of CO_2 anion which is a one-electron reduction process. In this section, we study the CO_2 adsorption on TiB_2 ML. Since 2D TMBs exhibit an atomic structure asymmetric along the z-direction therefore it is imperative to assess and compare the CO_2 adsorption ability on both surfaces like B surface (B_s) and TM surface (TM_s), which settle the active sites for CO_2 reduction process. On both surfaces, we have tried various possible configurations for CO_2 adsorption i.e. at top of TM/B, and hollow site (hcp), and

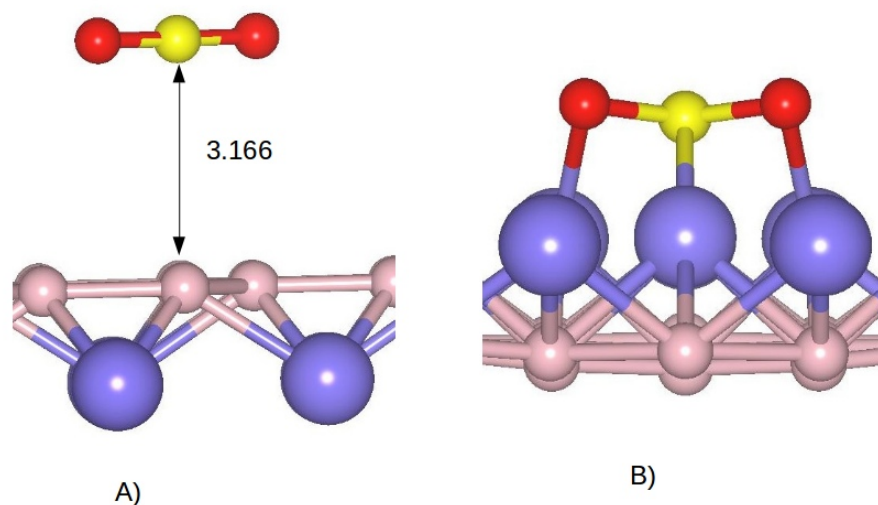


Figure 3.4: Side view of most stable configurations from the Ti and B side of TiB₂ monolayer. A) is the most stable configuration of CO₂ adsorption on TiB₂ ML from the Boron atom layer side and B) represents CO₂ adsorption at the hollow site from the Ti side (The distance in the figure is in Angstroms)

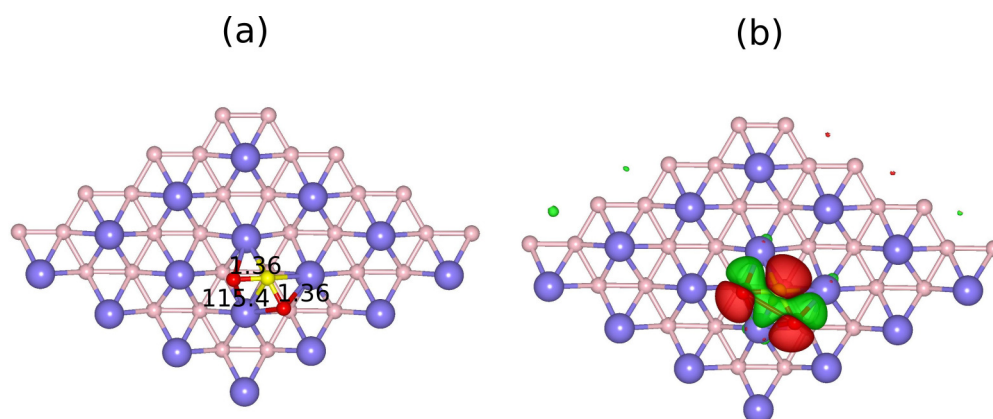


Figure 3.5: (a) The most stable configuration of adsorbed CO₂ on TiB₂, where bond lengths and angle are given in Å and (°). The purple, pink, yellow, and red spheres represent Ti, B, C, and O atoms. (b) The CDD diagram, where red and green regions represent the electron accumulation and depletion, respectively. The isosurface value is 0.008 e/Å⁻³

Table 3.2: The calculated E_{ads} , bond length (l_{C-O}), bond angle (θ , in degree) and charge transfer (CT) values of adsorbed CO_2 molecule on TiB_2 ML. The bond length is given in Å.

ML	E_{ads}	C-O	Ti/B-C	Ti/B-O	$\theta(^{\circ})$	CT
TiB_2 (Ti_s)	-2.47	1.36/1.36	2.18	2.20	115.42	1.76
TiB_2 (B_s)	-0.11	1.17	3.16	3.8	179.106	0.24

the corresponding relaxed geometries are shown in 3.4.

The most stable configurations of adsorbed CO_2 on TMBs surfaces are shown in Fig. 3.4 and adsorption energy with related parameters are listed in Table 3.2 for both surfaces. On TiB_2 ML, CO_2 molecule physisorbed on B_s with an adsorption energy of -0.11 eV while on TM_s surface CO_2 binds with bent geometry where the adsorption energy is -2.47 eV. It is noted that the adsorption of the CO_2 on the TM_s is energetically more favorable than the B_s surface thus, the detailed reaction pathways are systematically investigated only on the TM_s surfaces. In this configuration the C of CO_2 binds with the three nearest Ti atoms of the surface with the bond length of 2.18 Å. The O atoms bind with Ti atoms with two different bond lengths of 2.18 Å and 2.20 Å. The C-O bond length is 1.36 Å and the O-C-O bond angle is 115.12°.

We have plotted charge density difference (CDD) diagrams for adsorbed CO_2 as shown in Fig 3.5. The charge depletion region (red color) on the nearest Ti atoms and charge accumulation (blue color) on the CO_2 indicate that the TM_s surface act as a charge donor. Further, from bader charge [9] analysis we find that net total charge 1.76e is transferred from surrounding Ti atoms to the CO_2 molecule.

3.0.3 CO_2 to HCOOH pathways

In this section, the conversion of CO_2 to HCOOH (Formic acid) pathways will be explored. It is a two-electron reduction process that was first performed by Norskov et al [33]. The most prominent products in two-electron pathways are HCOOH and CO. After the activation of CO_2 on the catalyst surface, there are two types of hydrogenation possible on $*CO_2$. Proton can be added on either carbon or oxygen atom of adsorbed CO_2 . The first electron-proton transfer step performed on $*CO_2$ produces two intermediates $*COOH$ and $*HCOO$. We assume that the electron and proton transfer occurs simultaneously. Protonation at carbon atom gives $*HCOO$ and adding hydrogen on oxygen atoms results in $*COOH$ intermediate. The second electron-proton transfer step performed on the above two intermediates will give the successive intermediates. Two kinds of substitutions are possible at $*COOH$. Hydrogenation at the oxygen atom results in the formation of the $*CO$ with the release of a H_2O

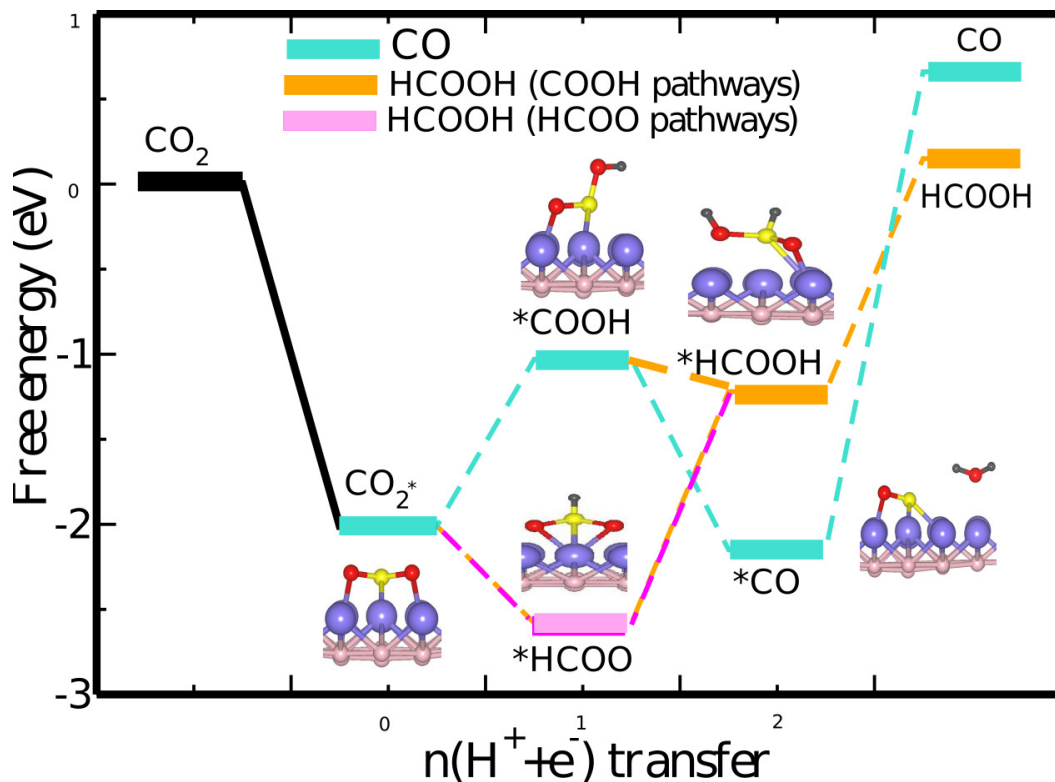


Figure 3.6: HCOOH pathway on TiB₂ surface

molecule ($*\text{COOH} + \text{H}^+ + \text{e}^- \leftrightarrow * \text{CO} + \text{H}_2\text{O}$) while protonation at C atom gives rise to $*\text{HCOOH}$ intermediate. Hydrogenation on $*\text{HCOO}$ gives only $*\text{HCOOH}$.

To explain the thermodynamics involved in the mechanism of the CO₂RR to Formic acid and CO pathways, we have plotted the relative free energy diagram as shown in Fig 3.6, where the total energy of pristine TiB₂(ML) + CO₂ + H₂ in the gaseous phase is taken as reference energy. As shown in Fig. 3.6, the formation of CO from CO₂ proceeds along $*\text{CO}_2 \rightarrow * \text{COOH} \rightarrow * \text{CO} \rightarrow \text{CO}$. After the CO₂ activation the formation of $*\text{COOH}$ requires the ΔG of 0.93eV(endothermic). Then the $*\text{CO}$ from $*\text{COOH}$ is an exothermic process with a $\Delta\text{G}=-1.12$ eV and further CO desorption is an uphill process with high $\Delta\text{G}(1.5$ eV). The high value of ΔG indicates a poor CO generation performance. Further, in this process($*\text{CO}_2 \rightarrow \text{CO}$), the stabilization of $*\text{CO}$ intermediate makes the desorption process difficult as a result desorption of CO is the potential determining step (PDS).

In the generation of HCOOH, there are two possible pathways i.e. $*\text{CO}_2 \rightarrow * \text{COOH} \rightarrow * \text{HCOOH} \rightarrow \text{HCOOH}$ (COOH pathways) and $*\text{CO}_2 \rightarrow * \text{HCOO} \rightarrow * \text{HCOOH} \rightarrow \text{HCOOH}$ (HCOO pathways) (Fig. 3.6). After the activation of $*\text{CO}_2$, the formation of $*\text{COOH}$ is an uphill process, and further $*\text{COOH} \rightarrow * \text{HCOOH}$ step is downhill with a ΔG of **-0.13 eV**, followed by a high ΔG of **0.56 eV** for the HCOOH desorption. As shown in Fig

3.6, the formation of $^*\text{HCOO}$ is easier than $^*\text{COOH}$ with ΔG of -0.56 eV although further hydrogenation of $^*\text{COOH}$ is not favorable due to the high value of ΔG 1.56 eV . Hence from free energy pathways, we find that the formic acid formation process would be favorable along the COOH pathways where the potential determining step is $^*\text{CO}_2 \rightarrow ^*\text{COOH}$.

3.0.4 Methanol Pathway

From the above two-electron pathway, we got a clear picture that $^*\text{CO}$ is very less likely to get desorbed due to high desorption energy hence, we can reduce it further to products like methanol and methane. The methanol pathway is a six-electron pathway that is a continuation of the formic acid pathway. $^*\text{CHO}$ is possible from both $^*\text{HCOOH}$ and $^*\text{CO}$. $^*\text{COH}$ is another possible intermediate by hydrogenation at the oxygen of $^*\text{CO}$ but this step is energetically expensive with a large barrier of (2.69eV). To get $^*\text{CHO}$ from $^*\text{CO}$, the electron-proton transfer step requires an external potential of (0.43eV) which is considerably lesser compared to $^*\text{COH}$. Hence, the formation of $^*\text{CHO}$ is a more stable intermediate. For the next step, hydrogenation at C and O of $^*\text{CHO}$ will give $^*\text{CH}_2\text{O}$ and CHOH respectively. $^*\text{CHO} + (\text{H}^+ + \text{e}^-) \rightarrow ^*\text{CH}_2\text{O}$ requires ΔG of 0.15eV while $^*\text{CHO} + (\text{H}^+ + \text{e}^-) \rightarrow ^*\text{CHOH}$ requires ΔG of 1.58eV externally. $^*\text{CH}_2\text{O}$ is thermodynamically more favourable due to the presence π^* orbital of C=O. The interaction between the neighboring Ti atoms and the empty π^* orbital makes it a stable intermediate compared to $^*\text{CHOH}$. In the 4th step, $^*\text{CH}_2\text{OH}$ is the possible intermediate from $^*\text{CHOH}$. $^*\text{CH}_3\text{O}$ and $^*\text{CH}_2\text{OH}$ are possible by hydrogenation at H and C of $^*\text{CH}_2\text{O}$ respectively. The most stable conformer of $^*\text{CH}_2\text{OH}$ is shown in Fig. 3.7. $^*\text{CH}_2^*\text{O} \rightarrow \text{CH}_2\text{OH}$ is an uphill process with ΔG of 1.11eV. The final electron-proton step gives $^*\text{CH}_3\text{OH}$ from $^*\text{CH}_3\text{O}$ and $^*\text{CH}_2\text{OH}$. $^*\text{CH}_3\text{O}$ is attached with TiB_2 surface from oxygen end as shown in Fig. 3.7. The external potential of 0.12 eV for ($^*\text{CH}_2^*\text{OH} \rightarrow \text{CH}_3\text{OH}$) while for ($^*\text{CH}_3^*\text{O} \rightarrow \text{CH}_3\text{OH}$) step 1.71 eV. The desorption energy for obtaining methanol is 0.32eV. Considering, the barriers associated with each electron-proton transfer step we can state that $^*\text{CHO} \rightarrow \text{CH}_2\text{O} \rightarrow \text{CH}_2\text{OH} \rightarrow \text{CH}_3\text{OH}$ is a thermodynamically most preferable pathway for methanol generation using TiB_2 ML as a catalyst. The PDS for the methanol pathway is $\text{CH}_2\text{O} \rightarrow \text{CH}_2\text{OH}$ step due to the ΔG_{max} of 1.11eV.

3.0.5 CH_4 Pathways

CH_4 is an 8 electron-proton transfer pathway. From, the intermediate $^*\text{CHOH}$ in previous methanol pathways the hydrogenation at the oxygen atom of the intermediate will give $^*\text{CH}$ with the release of the water molecule. Further, $^*\text{CH}_2\text{OH}$ intermediate form from $^*\text{CHOH}$ or $^*\text{CH}_2\text{O}$ as explained in previous pathways can give $^*\text{CH}_2$ if hydrogenated at oxygen with

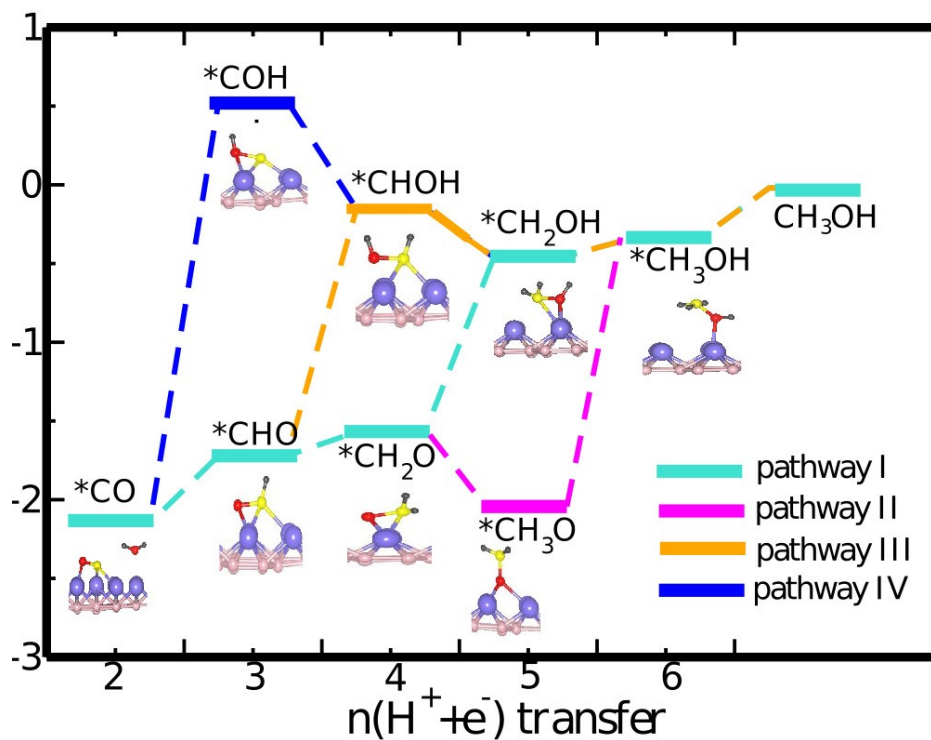


Figure 3.7: The free energy diagrams of CO₂RR to CH₃OH and corresponding intermediate configurations on TiB₂ ML.

the release of a water molecule. In a similar fashion *CH₃ is formed from *CH₃OH. Finally, *CH₄ is formed from *CH₃ by doing the final electron-proton transfer step. The distance of *CH₄ is 3.7Å which indicates loose interaction of CH₄ molecule with TiB₂.

From the Free energy diagrams, we derive the U_L values for CO, HCOOH, CH₃OH, and CH₄. U_L values came out to be -2.38, 1.1, 1.11, and 1.11 eV respectively. Some of the previous studies have reported that the initial step involving the adsorption of CO₂ is the most difficult step in CO₂RR. In our case, TiB₂ is showing excellent CO₂ adsorption on TiB₂ is showing excellent adsorption with an adsorption energy of -2.47eV. From the U_L values it's clear that among CO and HCOOH, HCOOH is the more favored product. At last, we also calculated U_L value for HER which turns out to be -0.49eV. The U_L value of HER is more than that of all the CO₂RR steps which indicates that HER reaction will occur before the CO₂RR steps. Hence, TiB₂ ML is facilitating the HER reaction as well with the CO₂RR pathways.

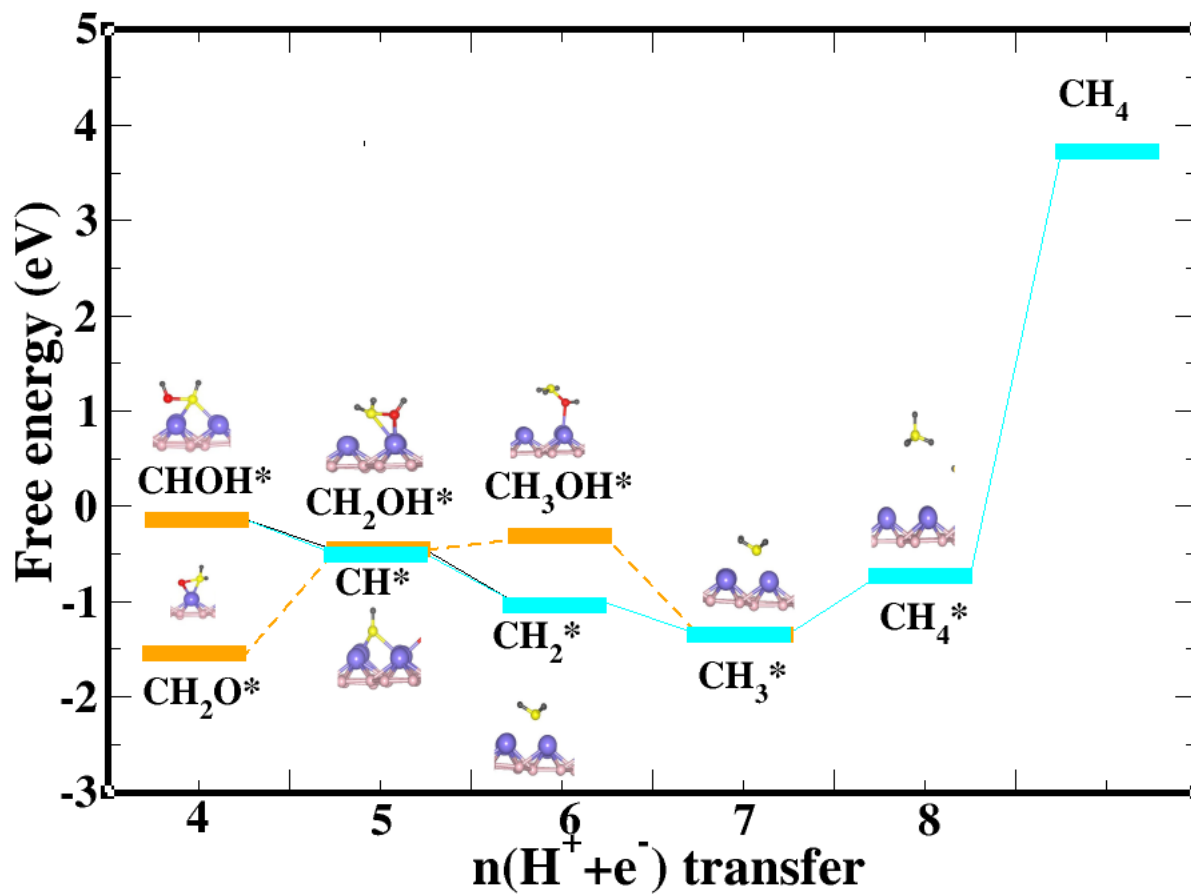


Figure 3.8: The free energy diagrams of CO₂RR to CH₄ and corresponding intermediate configurations on TiB₂ ML.

Chapter 4

Future Directions

4.0.1 Conclusion

We successfully studied the three pathways HCOOH, CH₃OH and CH₄ computationally and studied the interaction with TiB₂ ML. we also found the U_l value for the HER reaction on TiB₂ ML and we got $U_l = -0.49\text{eV}$. After comparing the U_l values we concluded the pristine surface is unable to suppress the HER reaction whereas it is actually supporting the HER reaction. We got excellent CO₂ adsorption on TiB₂ ML as we discussed earlier which is one of the supporting indicators for CO₂RR but at the same time a good catalyst for CO₂RR should suppress the HER which is happening with the combination and conditions used by us. Although it is a positive indicator to study HER applications as well on TiB₂ surface. This give rise to the various possibilities and schemes which and be implicated on our present computational model to resolve the issue of successfully the HER which is the prominent competitive reaction in CO₂RR.

4.0.2 Future Directions

Here, TiB₂ monolayer was used to study the CO₂RR. We got an idea of how the extent of CO₂RR depends on the active site on the catalyst and the contribution of active centers in better adsorption of the adsorbent(CO₂) on the catalyst. In the stipulated time of the project, we used a simplified model which we studied and there is scope for the inclusion of several parameters and reaction conditions which will strengthen the results. To be able to demonstrate the catalyst ready to try out for practical purposes further investigations can be done on our system.

4.0.3 Solvent Effect

In a practical situation, for an electrochemical reaction takes place there is a need for a solvent or an electrolyte. It is possible to create an atmosphere of dielectric around the surface using the self-consistent continuum solvation (SCCS) model. In our calculations, we can further take into account the effect of the solvent correction. Including the solvent corrections can create the hypothetical surrounding of the presence of the specific solvent.[2] The nature of solvent has the ability to affect the CO₂RR cycle considerably and can have a considerable say in the extent of adsorption of CO₂ and on further hydrogenation steps of CO₂.

4.0.4 External Potential

We know that providing external potential facilitates the amount of product formation. We have not included the effect of external potential in our pathways studies. It's important to witness the changes in pathways caused due to external potential. By including the External potential we can calculate the Gibbs Free Energy by the equation $\Delta G = -nFE$ where F is the Faradaic constant and E is the external potential.[34] Also, in a practical scenario, the reaction will not happen at pH=0 which we have considered. So, we can include the pH correction also. $\Delta G = -kT\ln[H^+]$ where k is the Boltzmann constant, T is temperature, and H⁺ are the hydrogen ions present in the system.

4.0.5 Doping

From the DOS plot of TiB₂, we can infer that the hexagonal boron lattice is almost inert throughout the reaction pathways. Hence, doping replacing the boron atom with appropriate TM can create the single atom catalyst active site(SACs) which have shown commendable performance in CO₂RR in the previous studies.

Bibliography

- [1] J Albo, M Alvarez-Guerra, P Castaño, and A Irabien. Towards the electrochemical conversion of carbon dioxide into methanol. *Green Chemistry*, 17(4):2304–2324, 2015.
- [2] Oliviero Andreussi, Ismaila Dabo, and Nicola Marzari. Revised self-consistent continuum solvation in electronic-structure calculations. *The Journal of chemical physics*, 136(6):064102, 2012.
- [3] B Basu, GB Raju, and AK Suri. Processing and properties of monolithic tib2 based materials. *International materials reviews*, 51(6):352–374, 2006.
- [4] Olga A Baturina, Qin Lu, Monica A Padilla, Le Xin, Wenzhen Li, Alexey Serov, Kateryna Artyushkova, Plamen Atanassov, Feng Xu, Albert Epshteyn, et al. Co2 electroreduction to hydrocarbons on carbon-supported cu nanoparticles. *ACS catalysis*, 4(10):3682–3695, 2014.
- [5] A. D. Becke. Density-functional exchange-energy approximation with correct asymptotic behavior. *Phys. Rev. A*, 38:3098–3100, Sep 1988.
- [6] Yu Chen, Chong Liu, Shien Guo, Tiancheng Mu, Lei Wei, and Yanhong Lu. Co2 capture and conversion to value-added products promoted by mxene-based materials. *Green Energy & Environment*, 7(3):394–410, 2022.
- [7] Ikhlas Ghiat and Tareq Al-Ansari. A review of carbon capture and utilisation as a co2 abatement opportunity within the ewf nexus. *Journal of CO2 Utilization*, 45:101432, 2021.
- [8] P Giannozzi, O Andreussi, T Brumme, O Bunau, M Buongiorno Nardelli, M Calandra, R Car, C Cavazzoni, D Ceresoli, M Cococcioni, N Colonna, I Carnimeo, A Dal Corso, S de Gironcoli, P Delugas, R A DiStasio Jr, A Ferretti, A Floris, G Fratesi, G Fugallo, R Gebauer, U Gerstmann, F Giustino, T Gorni, J Jia, M Kawamura, H-Y Ko, A Kokalj, E Küçükbenli, M Lazzeri, M Marsili, N Marzari, F Mauri, N L Nguyen, H-V Nguyen,

- A Otero de-la Roza, L Paulatto, S Poncé, D Rocca, R Sabatini, B Santra, M Schlipf, A P Seitsonen, A Smogunov, I Timrov, T Thonhauser, P Umari, N Vast, X Wu, and S Baroni. Advanced capabilities for materials modelling with Quantum ESPRESSO. *Journal of Physics: Condensed Matter*, 29(46):465901, 2017.
- [9] Graeme Henkelman, Andri Arnaldsson, and Hannes Jónsson. A fast and robust algorithm for bader decomposition of charge density. *Computational Materials Science*, 36(3):354 – 360, 2006.
- [10] R. L. Keiter J. E. Huheey, E. A. Keiter and O. K. Medhi. *Inorganic Chemistry*. Pearson Education India, 4 edition, 2006.
- [11] Abdolreza Javadi, Shuaihang Pan, Chezheng Cao, Gongcheng Yao, and Xiaochun Li. Facile synthesis of 10 nm surface clean TiO_2 nanoparticles. *Materials Letters*, 229:107–110, 2018.
- [12] Lei Ji, Le Chang, Ya Zhang, Shiyong Mou, Ting Wang, Yonglan Luo, Zhiming Wang, and Xuping Sun. Electrocatalytic CO_2 reduction to alcohols with high selectivity over a two-dimensional $\text{Fe}_2\text{P}_2\text{S}_6$ nanosheet. *ACS Catalysis*, 9(11):9721–9725, 2019.
- [13] Wolfram Koch and Max C Holthausen. *A chemist’s guide to density functional theory*. John Wiley & Sons, 2015.
- [14] W. Kohn and L. J. Sham. Self-consistent equations including exchange and correlation effects. *Phys. Rev.*, 140(4A):A1133–A1138, 1965.
- [15] Cong Liu, Haiying He, Peter Zapol, and Larry A Curtiss. Computational studies of electrochemical CO_2 reduction on subnanometer transition metal clusters. *Physical Chemistry Chemical Physics*, 16(48):26584–26599, 2014.
- [16] Hendrik J. Monkhorst and James D. Pack. Special points for brillouin-zone integrations. *Phys. Rev. B*, 13:5188–5192, Jun 1976.
- [17] Stephen Pacala and Robert Socolow. Stabilization wedges: solving the climate problem for the next 50 years with current technologies. *science*, 305(5686):968–972, 2004.
- [18] Robert G Parr. Density functional theory of atoms and molecules. In *Horizons of Quantum Chemistry: Proceedings of the Third International Congress of Quantum Chemistry Held at Kyoto, Japan, October 29–November 3, 1979*, pages 5–15. Springer, 1980.

- [19] M. C. Payne, M. P. Teter, D. C. Allan, T. A. Arias, and J. D. Joannopoulos. Iterative minimization techniques for ab initio total-energy calculations: molecular dynamics and conjugate gradients. *Rev. Mod. Phys.*, 64:1045–1097, Oct 1992.
- [20] MC Payne, MP Teter, DC Allen, and TA Arias. 1. d. joannopoulos, r, ev. *Mod. Phys*, 64:1045, 1992.
- [21] John P. Perdew, Kieron Burke, and Matthias Ernzerhof. Generalized gradient approximation made simple. *Phys. Rev. Lett.*, 77:3865–3868, Oct 1996.
- [22] Mar Pérez-Fortes, Jan C Schöneberger, Aikaterini Boulamanti, and Evangelos Tzimas. Methanol synthesis using captured co2 as raw material: Techno-economic and environmental assessment. *Applied Energy*, 161:718–732, 2016.
- [23] Jinli Qiao, Yuyu Liu, Feng Hong, and Jiujuun Zhang. A review of catalysts for the electroreduction of carbon dioxide to produce low-carbon fuels. *Chemical Society Reviews*, 43(2):631–675, 2014.
- [24] Muqing Ren, Hongzhi Zheng, Jincheng Lei, Jibo Zhang, Xiaojun Wang, Boris I Yakobson, Yan Yao, and James M Tour. Co2 to formic acid using cu–sn on laser-induced graphene. *ACS Applied Materials & Interfaces*, 12(37):41223–41229, 2020.
- [25] Muqing Ren, Hongzhi Zheng, Jincheng Lei, Jibo Zhang, Xiaojun Wang, Boris I. Yakobson, Yan Yao, and James M. Tour. Co2 to formic acid using cu–sn on laser-induced graphene. *ACS Applied Materials & Interfaces*, 12(37):41223–41229, 2020. PMID: 32830950.
- [26] GV Samsonov and BA Kovenskaya. Ii. the nature of the chemical bond in borides. *Boron and Refractory Borides*, pages 19–30, 1977.
- [27] Syed Shoaib Ahmad Shah, Muhammad Sufyan Javed, Tayyaba Najam, Costas Molochas, Naseem Ahmad Khan, Maowen Xu, Shujuan Bao, and Panagiotis Tsiakaras. Metal oxides for the electrocatalytic reduction of carbon dioxide active sites, composites, interface and defect engineering strategies. *Composites, Interface and Defect Engineering Strategies*.
- [28] Lu Jeu Sham and Walter Kohn. One-particle properties of an inhomogeneous interacting electron gas. *Physical Review*, 145(2):561, 1966.
- [29] Zhehao Sun, Hang Yin, Kaili Liu, Shuwen Cheng, Gang Kevin Li, Sibudjing Kawi, Haitao Zhao, Guohua Jia, and Zongyou Yin. Machine learning accelerated calculation and design of electrocatalysts for co2 reduction. *SmartMat*, 3(1):68–83, 2022.

- [30] David Vanderbilt. Soft self-consistent pseudopotentials in a generalized eigenvalue formalism. *Phys. Rev. B*, 41:7892–7895, 1990.
- [31] CJO Verzijl, JS Seldenthuis, and JM Thijssen. Applicability of the wide-band limit in dft-based molecular transport calculations. *The Journal of chemical physics*, 138(9):094102, 2013.
- [32] Xiaofei Wei, Shuxian Wei, Shoufu Cao, Yuying Hu, Sainan Zhou, Siyuan Liu, Zhaojie Wang, and Xiaoqing Lu. Cu acting as fe activity promoter in dual-atom cu/fe-nc catalyst in co₂rr to c₁ products. *Applied Surface Science*, 564:150423, 2021.
- [33] Jong Suk Yoo, Rune Christensen, Tejs Vegge, Jens K Nørskov, and Felix Studt. Theoretical insight into the trends that guide the electrochemical reduction of carbon dioxide to formic acid. *ChemSusChem*, 9(4):358–363, 2016.
- [34] Jong Suk Yoo, Rune Christensen, Tejs Vegge, Jens K Nørskov, and Felix Studt. Theoretical insight into the trends that guide the electrochemical reduction of carbon dioxide to formic acid. *ChemSusChem*, 9(4):358–363, 2016.
- [35] Ahmed Yousaf, Matthew S Gilliam, Shery LY Chang, Mathias Augustin, Yuqi Guo, Fraaz Tahir, Meng Wang, Alexandra Schwindt, Ximo S Chu, Duo O Li, et al. Exfoliation of quasi-two-dimensional nanosheets of metal diborides. *The Journal of Physical Chemistry C*, 125(12):6787–6799, 2021.
- [36] Ahmed Yousaf, Matthew S Gilliam, Shery LY Chang, Mathias Augustin, Yuqi Guo, Fraaz Tahir, Meng Wang, Alexandra Schwindt, Ximo S Chu, Duo O Li, et al. Exfoliation of quasi-two-dimensional nanosheets of metal diborides. *The Journal of Physical Chemistry C*, 125(12):6787–6799, 2021.
- [37] Chunmei Zhang, Tianwei He, Sri Kasi Matta, Ting Liao, Liangzhi Kou, Zhongfang Chen, and Aijun Du. Predicting novel 2d mb₂ (m= ti, hf, v, nb, ta) monolayers with ultrafast dirac transport channel and electron-orbital controlled negative poisson’s ratio. *The journal of physical chemistry letters*, 10(10):2567–2573, 2019.
- [38] Jincheng Zhang, Weizheng Cai, Fang Xin Hu, Hongbin Yang, and Bin Liu. Recent advances in single atom catalysts for the electrochemical carbon dioxide reduction reaction. *Chemical Science*, 12(20):6800–6819, 2021.
- [39] L. Z. Zhang, Z. F. Wang, S. X. Du, H.-J. Gao, and Feng Liu. Prediction of a dirac state in monolayer tib₂. *Phys. Rev. B*, 90:161402, 2014.

- [40] Congcong Zhao, Xiaofang Su, Shuo Wang, Yu Tian, Likai Yan, and Zhongmin Su. Single-atom catalysts on supported silicomolybdic acid for co₂ electroreduction: a dft prediction. *Journal of Materials Chemistry A*, 10(11):6178–6186, 2022.
- [41] Shuo Zhao, Renxi Jin, and Rongchao Jin. Opportunities and challenges in co₂ reduction by gold-and silver-based electrocatalysts: from bulk metals to nanoparticles and atomically precise nanoclusters. *ACS energy letters*, 3(2):452–462, 2018.